

Physics-Guided Graph Neural Networks for Floating Offshore Wind Turbine Wake Prediction

Mingqiu Liu¹, Jinguang Wang², Maokun Ye¹, Decheng Wan^{1*}

¹Computational Marine Hydrodynamics Lab (CMHL), School of Naval Architecture, Ocean and Civil Engineering, Shanghai Jiao Tong University, Shanghai, China

²Zhongnan Engineering Corporation Limited, Changsha, China

*Corresponding Author

ABSTRACT

The offshore wind power industry has developed significantly, with growing attention on floating offshore wind turbines (FOWTs) to harness wind energy resources in deep-sea regions. Predicting the wake structure of FOWTs is crucial for optimizing wind farm layouts, forecasting annual energy production, and enhancing overall wind farm efficiency. The additional motions of floating platforms introduce complex dynamics that substantially affect wake characteristics, making the wake structure more intricate and difficult to predict. This study uses Large Eddy Simulation (LES) coupled with the Actuator Line Model (ALM) to simulate the wake flow field of FOWTs under various wave conditions and analyzes the correlation between the wake structure, wave conditions, and motion responses. The results show that the velocity of the platform motion recovers in the accelerated wake region. Then, models are trained using simulation data, guided by physics, to predict the wake flow field of a FOWT under varying wave conditions. The models are validated against numerical data, demonstrating their ability to accurately predict the wake field. This study provides a potential solution for the rapid prediction of the FOWT wake flow field.

KEY WORDS: floating offshore wind turbine; wake prediction; graph neural networks; large eddy simulation.

INTRODUCTION

The wake effect can result in power losses in wind farms, with reductions of up to 40% (Fei et al., 2020). It also increases the fatigue loads on downstream wind turbines, thereby further impacting the overall power generation efficiency and operational costs. In recent years, floating offshore wind turbines (FOWTs) have garnered increasing attention due to their potential to harness the abundant wind energy resources in deep-sea areas (Chitteth Ramachandran et al., 2022). Compared to fixed-bottom wind turbines (FBWTs), FOWTs are installed on floating platforms and are subjected to wind, current, and wave loads, resulting in six degrees of freedom (DOF) motion, including surge, sway, heave, roll, pitch, and yaw. These motions enhance the mixing between the wake and the atmospheric boundary

layer turbulence, thereby influencing the wake distribution (Ramos-Garcia et al., 2022). Since the directions of wind, wave, and current loads are often closely aligned in real-world conditions, surge and pitch typically dominate the platform's motion and have garnered the most attention in related research (Subbulakshmi et al., 2022).

The study of FBWTs has progressed over several decades, yielding numerous well-established findings (Wang et al., 2024). As a result, much of the research on the wake prediction of FOWTs has been conducted based on the foundational understanding developed for FBWTs. Analytical wake models, such as Jensen model (Jensen, 1983) and Gaussian model (Bastankhah and Porté-Agel, 2014), are commonly used for wake prediction. Building upon these models, some researchers have developed analytical wake models specifically suited for FOWTs. Zhang et al. (2024) developed a 3D-OFWT wake model suitable for FOWTs through theoretical derivations based on the 3D Jensen-Gauss model. Zhang et al. (2024) proposed an analytical wake model specifically designed for pitch motion, building upon the Gauss model. Analytical wake models offer exceptionally high computational efficiency for predicting wind turbine wakes but are relatively limited in accuracy. Computational Fluid Dynamics (CFD) methods, including Large Eddy Simulation (LES) and Reynolds-Averaged Navier-Stokes (RANS), can provide comprehensive and highly accurate wake field data but come at the cost of significantly increased computational resources. Huang et al. (2023) investigated the wake interference between two FOWTs under different layouts using LES combined with the Unsteady Actuator Line Model (LES-UALM). Xu et al. (2024) employed LES-UALM to study the wake characteristics and aerodynamic responses of FOWT in atmospheric boundary layer conditions. Although CFD methods can provide high-accuracy data, their substantial computational costs make them challenging to apply on a large scale for wake prediction. Moreover, the simulation of FOWTs must account for wave conditions, which significantly amplifies computational demands. Achieving high-accuracy data while maintaining computational efficiency has become a significant challenge in this area of research.

The development of machine learning (ML) methods offers new possibilities for addressing this challenge. Many researchers have already applied these methods to the study of offshore wind turbines and demonstrated their feasibility (Masoumi, 2023). Machine learning

models can "learn" complex flow features from data, and they provide fast computational speed during the inference stage, making them highly suitable for tasks such as multi-parameter sensitivity analysis and rapid prediction. Purohit et al. (2022) compared the applicability of Support Vector Regression (SVR), Artificial Neural Networks (ANN), and Extreme Gradient Boosting (XGBoost) for predicting wind turbine wakes, using CFD-based datasets to train and validate their models. Li et al. (2023) utilized high-fidelity CFD simulation data to develop a Graph Neural Network (GNN) surrogate model, demonstrating that GNN can effectively capture complex flow features in wind turbine wakes. Furthermore, many researchers have integrated physical information or guidance into machine learning methods to better study physical phenomena, enhance training efficiency, and improve model credibility (Guo et al., 2022; Li et al., 2024; Gafoor Ctp et al., 2025). Combining machine learning with CFD-derived training data thus provides a promising approach to balancing accuracy and computational efficiency in wind turbine wake prediction. However, most existing studies focus on FBWTs, and efficiently and accurately predicting the wakes of FOWT remains an area requiring further investigation. To address this research gap, this study combines CFD with ML to achieve accurate and efficient predictions of FOWT wakes. The LES coupled with the Actuator Line Method (ALM) is employed to generate training data, while GNNs are utilized for wake prediction. Physical guidance is incorporated during the training process to enhance the models' rationality and efficiency. Finally, the results of the models are analyzed and validated.

METHODOLOGY

Large Eddy Simulation

The governing equations for LES, which account for the forces exerted by the wind turbine, Coriolis effects, and buoyancy, are as follows:

$$\frac{\partial \bar{u}_i}{\partial x_i} = 0 \quad (1)$$

$$\frac{\partial \bar{u}_i}{\partial t} + \frac{\partial (\bar{u}_i \bar{u}_j)}{\partial x_j} = -\frac{\partial \hat{p}}{\partial x_i} - \frac{\partial \tau_{ij}^D}{\partial x_j} - \frac{1}{\rho_0} \frac{\partial p_0(x, y)}{\partial x_i} + \frac{1}{\rho_0} F_i + g \left(\frac{\bar{\theta} - \theta_0}{\theta_0} \right) \delta_{i3} - \varepsilon_{i3k} f \bar{u}_k \quad (2)$$

where, the overbar denotes the spatially resolved components; t is time; u is the wind velocity; ρ_0 is the reference air density; τ_{ij}^D is the deviatoric part of the wind stress tensor; F_i represents the force exerted by the FOWT, which is calculated using ALM; g is the gravitational acceleration; ε_{ijk} is the alternating unit tensor; $\bar{\theta}$ is the resolved potential temperature; θ_0 is the reference temperature, set at 300 K; δ_{i3} is the Kronecker delta; f is the Coriolis parameter; and \hat{p} is the modified pressure, defined by $\hat{p} = (\bar{p} - p_0 + \rho g z) / \rho + \tau_{kk} / 3$, where, \bar{p} is the mean pressure; and p_0 is the static pressure.

The subgrid-scale model uses the Smagorinsky model (Smagorinsky, 1963). Based on this model, τ_{ij}^D is defined as $\tau_{ij}^D = -2(c_s \Delta)^2 |\bar{S}| \bar{S}_{ij}$, where, c_s is the Smagorinsky constant; $\bar{S}_{ij} = (\partial \bar{u}_i / \partial x_j + \partial \bar{u}_j / \partial x_i) / 2$ is the strain rate tensor after

filtration; and $|\bar{S}| = \sqrt{2\bar{S}_{ij}\bar{S}_{ij}}$ is the norm of the strain rate tensor. Further details on the governing equations can be found in Churchfield et al (2012).

Actuator Line Model

In CFD methods, directly modeling the blades of a wind turbine increases grid complexity and significantly consumes computational resources. Therefore, in studies of wind turbine wakes, blades are typically not modeled directly; instead, surrogate models are used to improve computational efficiency. The ALM is a widely used surrogate model (Sofensen and Shen, 2002). Its primary concept is to introduce a body force term into the governing equations to simulate the influence of the wind turbine on the flow field. This method simplifies the real turbine blades into a line composed of multiple actuator points. The body forces at these actuator points are calculated using blade element theory, with the corresponding formula as follows:

$$f = (L, D) = \frac{1}{2} \rho U_{rel}^2 c dr (C_L \mathbf{e}_L + C_D \mathbf{e}_D) \quad (3)$$

where, U_{rel} is the relative wind speed; L and D represent the lift and drag forces, respectively; ρ is the air density; c is the chord length; dr is the width of the blade element; C_L and C_D are the lift and drag coefficients, respectively; and \mathbf{e}_L and \mathbf{e}_D are the unit vectors of lift and drag, respectively.

Fig. 1 illustrates the velocity and force vectors acting on a blade element. In the figure, α represents the angle of attack, defined as the angle between the relative wind velocity and the chord line. The lift and drag coefficients are determined based on the angle of attack. The relative wind speed is the vector sum of the inflow wind speed, the rotational velocity of the blade, and the platform motion velocity. The formula is expressed as follows:

$$U_{rel} = U_\theta - \Omega r + U_z + U_M \quad (4)$$

where, U_θ and U_z are tangential and axial components of the inflow wind speed; Ω is the rotor speed; U_M is the platform motion velocity.

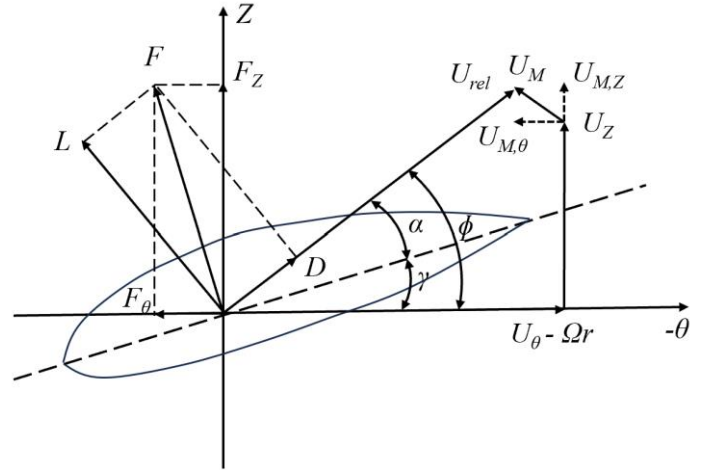


Fig. 1 velocity and force vectors of the blade element

To avoid numerical singularities, the body force needs to be smoothly distributed over the computational grid. The Gauss kernel function is typically used for this smoothing process. The smoothed body force is expressed as follows:

$$f_\varepsilon = f \otimes \eta_\varepsilon = \sum_{i=1}^N f_i(x_i, y_i, z_i, t) \frac{1}{\varepsilon^3 \pi^{3/2}} \exp \left[-\left(\frac{d_i}{\varepsilon} \right)^2 \right] \quad (5)$$

where, N is the number of the blade elements; x_i, y_i, z_i is the position of the blade element; d_i represents the distance between the mesh position and the blade element; ε is the projection width. The selection of the projection width can significantly influence the simulation results of wind turbine aerodynamic performance. It is generally set to a value of $\varepsilon = 2\Delta x$ (Xu et al., 2023), where Δx is the mesh size.

Graph Neural Networks

Graph Neural Networks (GNNs) have undergone significant development over the past decade (Scarselli et al., 2009) and have been applied in various domains, including physics simulations, traffic prediction, and graph generation (Zhou et al., 2020). In GNNs, a graph represents the relationships between nodes and edges, as illustrated in Fig. 2, where circles represent nodes and lines represent edges. GNNs excel at handling unstructured data. The input is a graph $G=(V,E)$, where $V \in \mathbb{R}^{n \times f}$ represents n nodes, each containing f features, and $E \in \mathbb{R}^{2 \times n_e}$ represents n_e edges, with each edge defined by the two vertices it connects. In GNNs, each node learns information from its own features and those of its neighbors (local information aggregation), enabling node-level prediction tasks. Through this training process, the forward propagation returns a graph with the same connectivity and updated node features. These updated node features are then used to perform the target prediction.

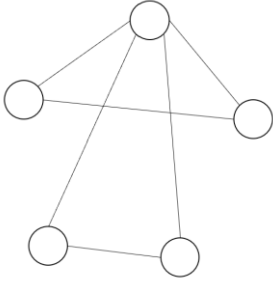


Fig. 2 “Graph” schematic diagram

Based on different mechanisms for updating node information, various GNN methods have been developed, including Graph Convolutional Networks (GCN), Graph Attention Networks (GAT), and GraphSAGE (Zhou et al., 2020). This study adopts the GAT framework because it introduces a self-attention mechanism that assigns different weights to each neighbor of a node, thereby highlighting the most critical neighbor information during aggregation. Compared to traditional methods, GAT is better suited to complex graph structures and enhances the model’s expressive power and prediction accuracy. The GAT update rule can be formulated as follows:

$$x_v^{(k)} = \bigoplus_{h=1}^H \sigma \left(\sum_{u \in N(v)} \alpha_{uv}^{(h)} W^{(h)} x_u^{(k-1)} \right) \quad (6)$$

where $N(v)$ is the neighborhood of node v , H is the number of attention heads, σ is the activation function, α_{uv} is the attention coefficient, $W^{(h)}$ is the weight matrix of h layer, and \bigoplus represents concatenation.

DATA PREPARATION AND MODEL TRAINING

Data Generation

In this study, the LES-ALM method is employed to simulate FOWT in the atmospheric boundary layer environment, generating high-fidelity wake data under wave conditions for subsequent GNN training. The solver used is SOWFA-FAST (Churchfield et al., 2012; Xu et al., 2023), which is an open-source software developed by National Renewable Energy Laboratory (NREL).

The simulation process consists of two steps. The first step is a precursor simulation to generate the atmospheric boundary layer flow field. The second step involves wind turbine simulation, where the flow field generated in the first step is used as input, and an FOWT model is introduced into the flow field to simulate wake dynamics and fully coupled behavior. Note that the high-resolution wake field is obtained using the LES-ALM method, while the fully coupled behavior is computed using FAST. The bidirectional coupling between FAST and ALM is achieved through SOWFA. Specifically, the LES-ALM framework solves the flow field and transfers the inflow wind velocity to FAST, which performs fully coupled dynamic simulations of the wind turbine. At the next time step, the wind turbine’s body forces and position are transferred back to the LES framework for continuous simulation.

The wind turbine used is the NREL 5MW turbine, with a rated wind speed of 11.4 m/s, a rated rotational speed of 12.1 rpm, a rotor diameter of 126 m, and a hub height of 90 m. Further details can be found in Jonkman et al (2009). The floating platform is a semi-submersible OC4 platform designed for a water depth of 200 m, with a top height of 10 m. Additional details are available in Robertson et al (2014).

The computational domain is designed as a rectangular region, as shown in Fig. 3, with dimensions of 3 km \times 1 km \times 1 km. The lateral boundaries are cyclic, the top boundary is slip, and the bottom boundary uses the Moeng model. The inflow direction aligns with the positive x-axis. The grid resolution for the precursor simulation is 10 m \times 10 m \times 10 m, with a simulation time of 19,000 s and a time step of 0.2 s. The first 18,000 s are used to establish the quasi-equilibrium atmospheric boundary layer flow field, and the final 1,000 s are used to generate inflow conditions for the wind turbine simulation. During the wind turbine simulation, mesh refinement is applied around the wind turbine and in the wake region to achieve accurate flow field results. The refined area is a rectangular region with two levels of refinement to avoid abrupt changes in grid size that could affect numerical simulation, as shown in Fig. 4. The heights of the two refinement zones are $2D$ and $3D$, respectively, where D is the rotor diameter. The grid size in the second refinement zone is 2.5 m \times 2.5 m \times 2.5 m, resulting in a total of 12 million grid cells. The wind turbine simulation is conducted for a duration of 1,000 seconds with a time step of 0.02 s. For additional simulation details, including grid convergence analysis and solver validation, refer to Xu et al (2023).

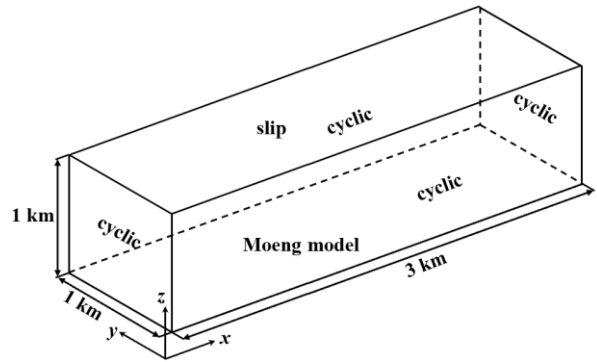


Fig. 3 Computational domain

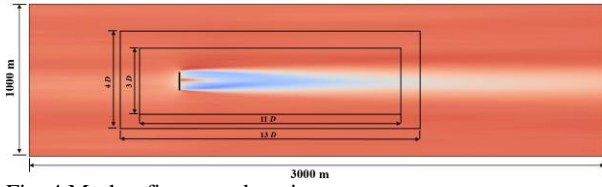


Fig. 4 Mesh refinement domain

The simulation uses an inflow wind speed of the rated value, 11.4 m/s. After the precursor simulation, the wind speed at hub height remained at 11.4 m/s, exhibiting an exponential distribution with height. The surface roughness is set to 0.001 m, and the atmospheric boundary layer is assumed to be neutral. The wave conditions are set as regular waves, referencing sea states corresponding to scale 6–8 as designed by Robertson et al (2014). The case settings are detailed in Table 1, where T and H represent the wave period and wave height, respectively. Case 1 corresponds to FBWT and is included for comparative analysis.

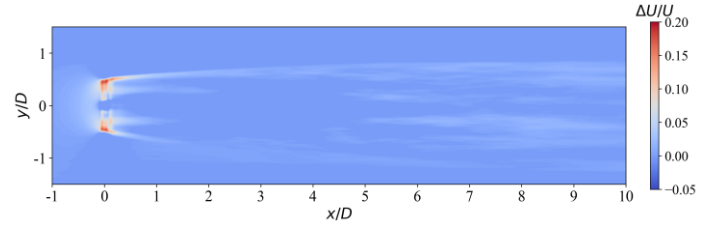
Table 1. Case settings

No.	T	H
1	0	0
2	11.3	5.49
3	13.6	9.14
4	17	15.24

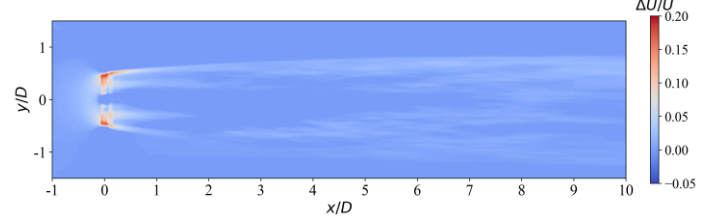
Correlation Analysis

This study conducts a correlation analysis of the simulation results to explore the relationships between key parameters and provide physical guidance for subsequent training. First, the differences in the wake structures of FOWTs under various wave conditions are analyzed based on numerical simulation results. The simulated wakes exhibit a progression from development to stabilization; therefore, the final 600 s of the stabilized wake are selected for analysis in this study. Fig. 5 illustrates the differences in time-average velocity deficits at the hub-height horizontal plane between the FBWT and the FOWT cases. The differences are calculated by subtracting the velocity deficits of the three FOWT cases from the corresponding velocity deficit of Case 1. From the figure, it can be observed that as the wave period and wave height increase, the velocity deficit at the same downstream location for the FOWT gradually decreases, indicating a faster wake recovery. This phenomenon is likely due to the increased platform motion response caused by higher wave periods and wave heights, which enhances the mixing between the wake and the atmospheric boundary layer, thereby accelerating wake recovery.

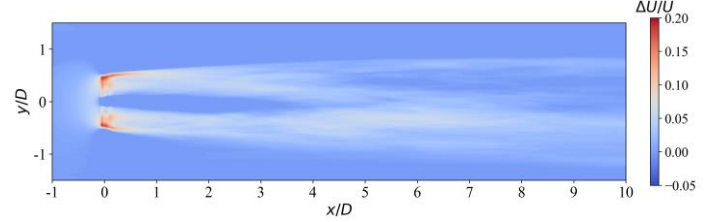
Fig. 6 shows the time-series variations of surge and pitch motion responses. The amplitudes of the motion responses in the other four degrees of freedom are relatively small and have a negligible impact on the overall dynamics; therefore, this study focuses primarily on the motion responses of these two degrees of freedom. As shown in the figure, the motion responses increase with rising wave periods and wave heights, which aligns with the observed trend of faster wake recovery under these conditions.



(a) Case1-2

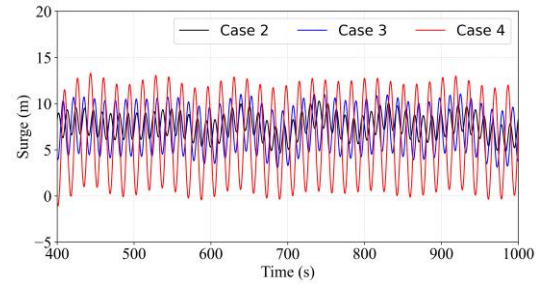


(b) Case1-3

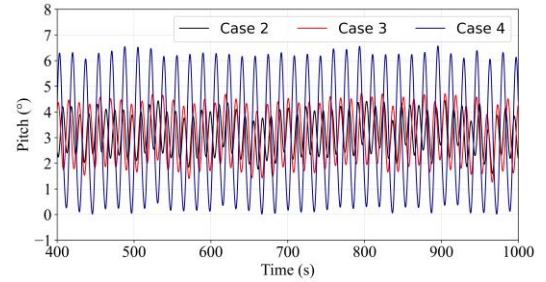


(c) Case1-4

Fig. 5 Velocity deficit difference map



(a) surge motion



(b) pitch motion

Fig. 6 Motion response

Next, frequency domain analysis is employed to examine the relationship between platform motion response and wake behavior. By performing a Fourier transform on the time history curves of the motion responses, the relationship between power spectral density (PSD) and frequency can be obtained. Fig. 7 shows the PSD of surge and pitch motions, with dashed lines from left to right representing the wave frequencies of $1/11.3$, $1/13.6$, and $1/17$. The figure reveals that the peaks in motion response energy correspond to their respective wave frequencies, indicating that the motion responses are primarily

influenced by wave action.

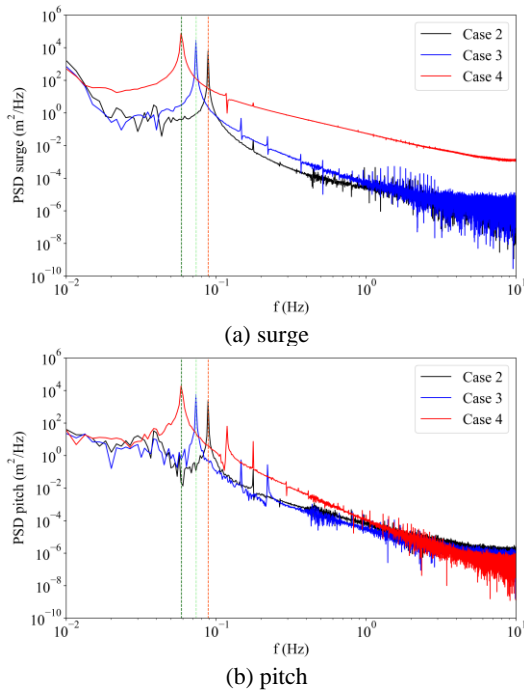


Fig. 7 Power spectrum density of motion response

Fig. 8 presents the PSD of the thrust force, where the dashed lines similarly indicate the wave frequencies. The figure shows that the frequency at which the thrust energy peaks align with the frequency of the motion response energy peaks, demonstrating a consistent relationship between motion response and thrust. Variations in thrust induce changes in the velocity distribution in the near-wake region, causing axial wake velocity oscillations at the same frequency (Fontanella et al., 2022). These oscillations further influence the velocity distribution in the far-wake region.

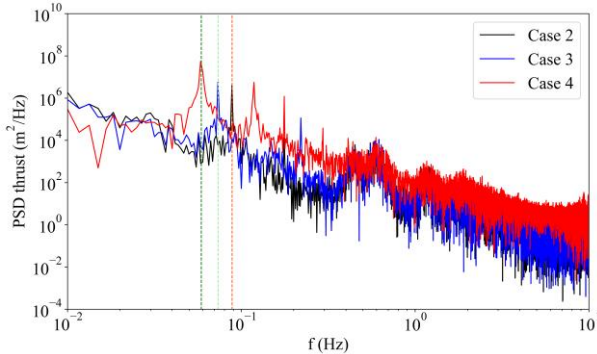


Fig. 8 Power spectrum density of thrust

Model definition and training

In this study, Multi-Layer Perceptrons (MLPs) are added to both the input and output ends of the GAT framework to enhance the overall representation and prediction capabilities of the model, as illustrated in Fig. 9. Specifically, the input MLP transforms raw input features by projecting them into a higher-dimensional embedding space through nonlinear mappings. This process increases the complexity and expressiveness of node features, thus making the input features more suitable for capturing spatial dependencies in the subsequent GAT

layers. During training, the parameters of the input MLP are optimized jointly with the GAT via gradient descent to minimize the prediction error. The output MLP then integrates and further transforms the high-dimensional node features produced by the GAT, projecting it back to the original dimension and thereby improving the model's predictive performance.

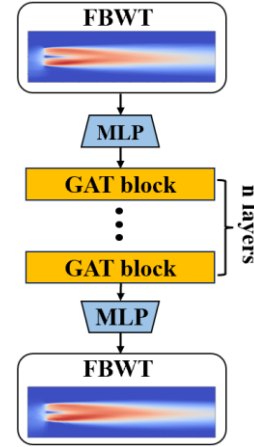


Fig. 9 network architecture

The training data is derived from CFD simulations, with the time-averaged data from the final 600 seconds used for training. The results are processed into grid-based velocity distribution data on the horizontal plane and vertical plane at the hub height. The input node features for training include the coordinates and velocity deficit information of the FBWT flow field. Additionally, key parameters influencing the FOWT wake, including wave period, wave height, and the amplitudes of surge and pitch motion responses, are incorporated as global information into the node features.

The adjacency matrix is generated based on the grid data to establish the adjacency relationships. To fully capture the flow field characteristics, each grid point is connected to its surrounding eight grid points. The output node features represent the velocities at the corresponding coordinates of the FOWT case under the given wave conditions. The GNNs consist of 5 layers with a hidden layer dimension of 64 and 2 attention heads. The MLP layers have a dimension of 32. The Adam optimizer is used, with the Mean Squared Error (MSE) as the loss function. The initial learning rate is set to 0.0001, and a dynamic learning rate adjustment is applied during training. Specifically, if the loss does not decrease for 20 consecutive steps, the learning rate is reduced to 10% of its current value. The training is performed on an NVIDIA GeForce RTX 4060 Ti, and the model is implemented using the open-source library PyTorch Geometric (Fey and Lenssen, 2019). The training results will be presented in the next section.

RESULTS AND DISCUSSION

Horizontal Plane Wake

The wake structure at the hub height level is the focal point of this research field. In this study, flow field maps on the horizontal plane obtained from Case 1, 2, and 4 simulations are used to train a model that can predict the FOWT wake field based on the FBWT flow field, wave parameters, and motion responses. Fig. 10 shows the curve of the loss function decreasing with each epoch. As observed in the figure, the training effectively reached an optimal state, and after a certain number of epochs, the model performance stabilized.

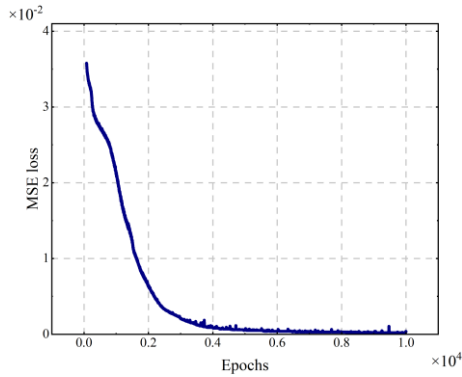


Fig. 10 Training MSE curve

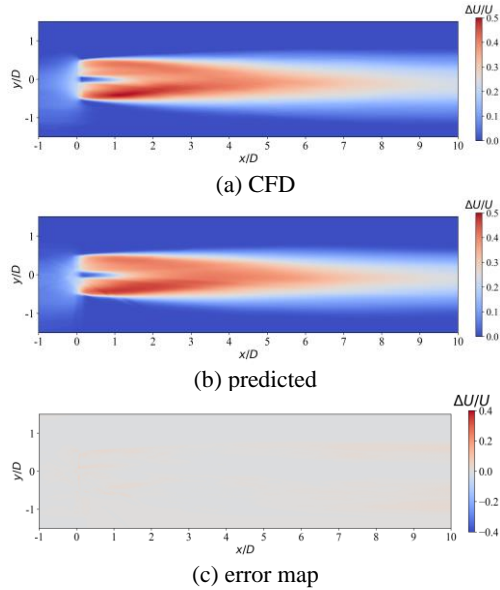


Fig. 11 CFD and predicted wake flow comparison for Case 2: horizontal plane

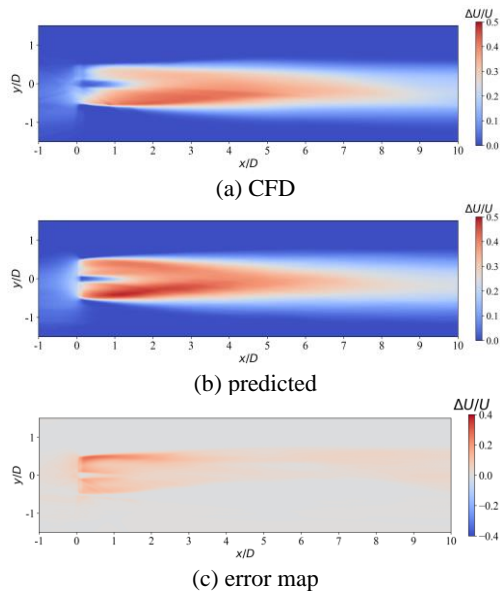


Fig. 12 CFD and predicted wake flow comparison for Case 3: horizontal plane

Fig. 11 presents a comparison between the CFD simulation results and the predicted results for Case 2. As shown in the figure, the model achieves good performance in predicting the FOWT wake in the training set, successfully capturing the flow features in the field. Additionally, the overall error is relatively small, with a MSE of $6e-5$.

This study uses Case 3, which is outside the training set, for validation. Fig. 12 presents a comparison between the CFD simulation results and the predicted results for Case 3. As shown in the figure, the model is able to predict the FOWT wake structure with reasonable accuracy. However, the overall error is slightly higher compared to the training set, with a MSE of $1.5e-3$. The region with larger errors is mainly concentrated in the near-wake zone. This may be due to the more complex wake structure in the near-wake region, which is heavily influenced by the wind turbine's interference, making it difficult for the model to learn such intricate physical phenomena.

Vertical Plane Wake

Studying the wake structure on the vertical plane at hub height helps to understand the variation characteristics of the FOWT wake at different heights. In this study, the flow field maps on the vertical plane obtained from simulations of Case 1, 2, and 4 are used to train a model that can predict the FOWT wake field based on the FBWT flow field, wave parameters, and motion responses. Fig. 13 shows the curve of the loss function decreasing with the number of epochs. From the figure, it can be seen that the model achieves a good fitting effect, and after sufficient iterations, its performance stabilizes.

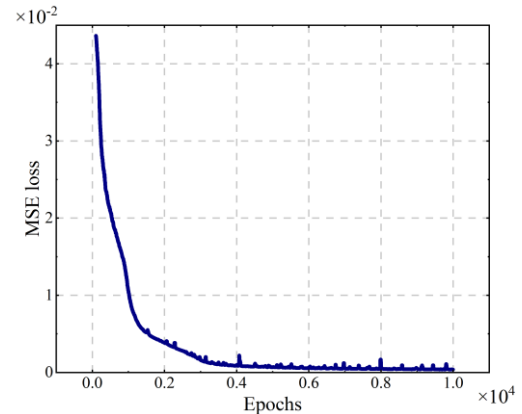


Fig. 13 Training MSE curve

Fig. 14 shows the comparison between the CFD simulation results and the predicted results for Case 2. From the figure, it can be seen that the model is also able to predict the FOWT wake effectively on the training set, capturing the vertical flow characteristics with a MSE of $9e-6$.

This study uses Case 3 for validation. Fig. 15 shows the comparison between the CFD simulation results and the predicted results for Case 3. From the figure, it can be seen that, overall, the model is able to predict the FOWT wake structure with a MSE of $3.5e-3$. However, the error is still relatively large in the near-wake region. Additionally, the error is also significant in the upper part of the wake, near the atmospheric boundary layer. This could be due to the complex mixing process between the wake and the atmospheric boundary layer under turbulent conditions, leading to certain errors when the model predicts this complex phenomenon.

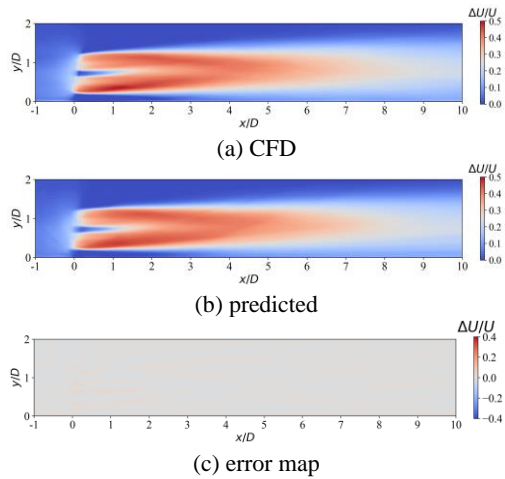


Fig. 14 CFD and predicted wake flow comparison for Case 2: vertical plane

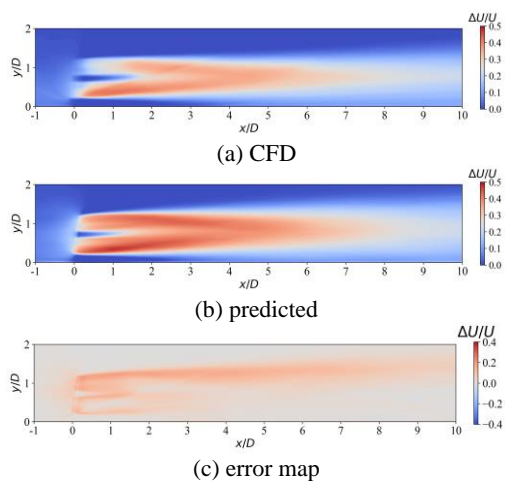


Fig. 15 CFD and predicted wake flow comparison for Case 3: vertical plane

CONCLUSIONS

This study aims to rapidly predict the wake flow field of a FOWT by extracting key spatial features of the flow field from FBWT flow field data using GAT, and combining wave parameters and motion response parameters. The LES-ALM method is employed to simulate the FBWT and FOWT under multiple wave conditions, followed by a physical analysis of the data. The results show that wave conditions, along with surge and pitch motion responses, affect the wake structure of the FOWT. Guided by physical insights, CFD simulation data is used as training data to develop a model that predicts the FOWT wake field based on the FBWT flow field, wave parameters, and surge and pitch motion responses. Validation is performed using conditions outside the training set, and the results indicate that the model can accurately predict the FOWT wake structure. However, some discrepancies are observed in the near-wake and wake boundary regions, which may be due to the significant influence of the wind turbine in the near-wake zone and the turbulent mixing between the wake boundary and the atmospheric boundary layer. These regions have complex flow structures that are challenging to capture.

By combining the accuracy of CFD with the efficiency of machine learning, this study significantly reduces computational effort, offering

rapid and effective predictions of FOWT wakes across various conditions. With an expanded training dataset, this method can be used as a surrogate model for the rapid prediction of FOWT flow fields. In the future, other machine learning methods such as CNN and RNN can be explored to evaluate the robustness of different approaches. Additionally, irregular wave conditions can be added to the training process to better adapt to real-world environments.

ACKNOWLEDGEMENT

This work is supported by the National Natural Science Foundation of China (52131102), to which the authors are most grateful.

REFERENCES

- Bastankhah, M, and Porté-Agel, F (2014). "A new analytical model for wind-turbine wakes," *Renewable Energy*, 70, 116–123.
- Chitteth Ramachandran, R, Desmond, C, Judge, F, Serraris, J-J, and Murphy, J (2022). "Floating wind turbines: marine operations challenges and opportunities," *Wind Energy Sci*, 7(2), 903–924.
- Churchfield, MJ, Lee, S, Michalakes, J, and Moriarty, PJ (2012). "A numerical study of the effects of atmospheric and wake turbulence on wind turbine dynamics," *Journal of Turbulence*, 13, N14.
- Fei, Z, Tengyuan, W, Xiaoxia, G, Haiying, S, Hongxing, Y, Zhonghe, H, Yu, W, and Xiaoxun, Z (2020). "Experimental study on wake interactions and performance of the turbines with different rotor-diameters in adjacent area of large-scale wind farm," *Energy*, 199, 117416.
- Fey, M, and Lenssen, JE (2019). "Fast Graph Representation Learning with PyTorch Geometric.,"
- Fontanella, A, Zasso, A, and Belloli, M (2022). "Wind tunnel investigation of the wake-flow response for a floating turbine subjected to surge motion," *J Phys: Conf Ser*, 2265(4), 042023.
- Gafoor Ctp, A, Kumar Boya, S, Jinka, R, Gupta, A, Tyagi, A, Sarkar, S, and Subramani, DN (2025). "A physics-informed neural network for turbulent wake simulations behind wind turbines," *Physics of Fluids*, 37(1), 015110.
- Guo, N-Z, Shi, K-Z, Li, B, Qi, L-W, Wu, H-H, Zhang, Z-L, and Xu, J-Z (2022). "A physics-inspired neural network model for short-term wind power prediction considering wake effects," *Energy*, 261, 125208.
- Huang, Y, Zhao, W, and Wan, D (2023). "Wake interaction between two spar-type floating offshore wind turbines under different layouts," *Physics of Fluids*, 35(9), 097102.
- Huanqiang, Z, Xiaoxia, G, Hongkun, L, Qiansheng, Z, Xiaoxun, Z, Yu, W, and Fei, Z (2024). "Investigation of a new 3D wake model of offshore floating wind turbines subjected to the coupling effects of wind and wave," *Applied Energy*, 365, 123189.
- Jensen, NO (1983). "A note on wind generator interaction", *Risø-M*. 2411.
- Jonkman, J, Butterfield, S, Musial, W, and Scott, G (2009). "Definition of a 5-MW Reference Wind Turbine for Offshore System Development.,"
- Li, B, Ge, M, Li, X, and Liu, Y (2024). "A physics-guided machine learning framework for real-time dynamic wake prediction of wind turbines," *Physics of Fluids*, 36(3), 035143.
- Li, S, Zhang, M, and Piggott, MD (2023). "End-to-end wind turbine wake modelling with deep graph representation learning," *Applied Energy*, 339, 120928.
- Masoumi, M (2023). "Machine Learning Solutions for Offshore Wind Farms: A Review of Applications and Impacts," *JMSE*, 11(10), 1855.

- Purohit, S, Ng, EYK, and Syed Ahmed Kabir, IF (2022). "Evaluation of three potential machine learning algorithms for predicting the velocity and turbulence intensity of a wind turbine wake," *Renewable Energy*, 184, 405–420.
- Ramos-García, N, Kontos, S, Pegalajar-Jurado, A, González Horcas, S, and Bredmose, H (2022). "Investigation of the floating IEA Wind 15 MW RWT using vortex methods Part I: Flow regimes and wake recovery," *Wind Energy*, 25(3), 468–504.
- Robertson, A, Jonkman, J, Masciola, M, Song, H, Goupee, A, Coulling, A, and Luan, C (2014). "Definition of the Semisubmersible Floating System for Phase II of OC4.,"
- Scarselli, F, Gori, M, Ah Chung Tsoi, Hagenbuchner, M, and Monfardini, G (2009). "The Graph Neural Network Model," *IEEE Trans Neural Netw*, 20(1), 61–80.
- Smagorinsky, J (1963). "GENERAL CIRCULATION EXPERIMENTS WITH THE PRIMITIVE EQUATIONS: I. THE BASIC EXPERIMENT*," *Mon Wea Rev*, 91(3), 99–164.
- Sofensen, JN, and Shen, WZ (2002). "Numerical Modeling of Wind Turbine Wakes," *Journal of Fluids Engineering*, 124(2), 393–399.
- Subbulakshmi, A, Verma, M, Keerthana, M, Sasmal, S, Harikrishna, P, and Kapuria, S (2022). "Recent advances in experimental and numerical methods for dynamic analysis of floating offshore wind turbines — An integrated review," *Renewable and Sustainable Energy Reviews*, 164, 112525.
- Wang, L, Dong, M, Yang, J, Wang, L, Chen, S, Duić, N, Joo, YH, and Song, D (2024). "Wind turbine wakes modeling and applications: Past, present, and future," *Ocean Engineering*, 309, 118508.
- Xu, S, Zhuang, T, Zhao, W, and Wan, D (2023). "Numerical investigation of aerodynamic responses and wake characteristics of a floating offshore wind turbine under atmospheric boundary layer inflows," *Ocean Engineering*, 279, 114527.
- Xu, S, Yang, X, Zhao, W, and Wan, D (2024). "Numerical analysis of aero-hydrodynamic wake flows of a floating offshore wind turbine subjected to atmospheric turbulence inflows," *Ocean Engineering*, 300, 117498.
- Zhang, P, Li, C, Wei, Y, and Wu, W (2024). "Three-dimensional analytical wake model for floating offshore wind turbines under pitch motion," *Ocean Engineering*, 311, 118935.
- Zhou, J, Cui, G, Hu, S, Zhang, Z, Yang, C, Liu, Z, Wang, L, Li, C, and Sun, M (2020). "Graph neural networks: A review of methods and applications," *AI Open*, 1, 57–81.